High-Power-Factor Single-Phase Diode Rectifier Driven by Repetitively Controlled IPM Motor

Kazuya Inazuma, Hiroaki Utsugi, Kiyoshi Ohishi, *Senior Member, IEEE*, and Hitoshi Haga, *Member, IEEE*

***Abstract*—This paper proposes a new power factor correction method using an inverter-driven interior permanent magnet (IPM) motor. The proposed system realizes the high power factor of a single-phase diode rectifier by using a three-phase pulsewidth modulation inverter and an IPM motor. The proposed converter consists of a single-phase diode rectifier, a small film capacitor at the dc link (14 μF and 0.33 J/kVA), a three-phase voltage-source inverter, and an IPM motor. In the proposed system, the inverter has the following two functions: 1) It regulates the velocity of the IPM motor, and 2) it controls the source-side-current waveform. In order to obtain a unity-power-factor operation at the source side, we propose and implement a new control method that regulates the inverter output power. The proposed control method is that the inverter regulates $d-q$-axis current synchronous with input voltage. An inverter-output-power controller is positioned between a speed controller and a q-axis current controller. The inverter output power is regulated by a proportional–integral and repetitive controller. The maximum power factor obtained by the proposed method is 98.7% at the rated-load conditions. The superior performance of the proposed system is demonstrated by experimental results.**

***Index Terms*—High power factor, interior permanent magnet (IPM) synchronous motor (IPMSM) drive, inverter, repetitive control.**

I. Introduction

VARIABLE-SPEED ac motor systems have been applied to home electrical appliances, from the viewpoint of alleviating global environmental problems [1]–[3]. In a residential air-conditioner application, controlling the compressor with a variable-speed motor drive would allow overall system optimization that could significantly reduce energy consumption. On the other hand, the demand for improving the power quality of the ac sources has become a great concern because of the rapidly increasing usage of these electrical appliances. In recent years, the variable-speed ac motor drive systems used in home electrical appliances are necessary for power factor correction (PFC) circuits. The primary goal is to achieve the reduction of harmonic contamination in the source side and the improvement of transmission efficiency. In this light, PFC research, which is a branch of power electronics, has attracted considerable attention. Conventional PFC requires the use of electrolytic capacitors, reactors, and switching devices. The electrolytic capacitors in the inverter circuit occupy a large volume; this prevents miniaturization of the circuit and limits its lifetime. Reactors and switching devices significantly contribute toward an increase in power loss, weight of the circuit, and its cost. In order to further conserve energy and resources of the motor drive system, PFC circuits have demanded high efficiency and the reduction of size and weight.

Numerous PFC topologies have been recently developed and reported in the literatures [4]–[17]. However, the PFC circuits in [4]–[6] must have isolation. The circuits in [7]–[10] obtain high efficiency. However, the PFC circuits require an additional reactor and switching devices. The circuits in [11]–[17] realize small size and high efficiency. On the contrary, the PFC circuits also require electrolytic capacitors, reactors, and switching devices. Hence, these conventional PFC circuits are not suitable for the economical motor drive system, which is applied in air-conditioners.

This paper proposes a new variable-speed motor drive system containing a three-phase interior permanent magnet (IPM) motor. The proposed system consists of a diode rectifier, a three-phase inverter, and a small film capacitor. The proposed power converter does not have energy storage. The dc-link capacitance is 14 μF (0.33 J/kVA). Hence, the source-side ripple power is smoothed at the moment of inertia of the IPM motor. Both the source-side power factor and the motor speed are controlled by the three-phase inverter. The motor speed is controlled averagely because the three-phase output power includes many ripple power synchronous with the single-phase source voltage. The torque ripple appears at the IPM motor. In particular, when the motor speed is the double frequency of the source frequency, the sound noise became large. The proposed system is useful for the compressor drive application.

In a previous report in [33], high-power-factor operation is obtained only at rated-load condition. The power factor was lower than 90% at light-load condition, because the q-axis current controller was not fine for the input power ripple with a frequency of 100 Hz. This paper proposes an inverter-control method for the single-phase-to-three-phase converter without an electrolytic capacitor, in order to obtain a high power factor and to achieve input-current-waveform improvements under light- and rated-load conditions. This proposed topology with

Manuscript received August 26, 2011; revised December 12, 2011 and February 29, 2012; accepted April 10, 2012. Date of publication July 19, 2012; date of current version May 16, 2013.

K. Inazuma was with the Department of Electrical Engineering, Nagaoka University of Technology, Nagaoka 940-2188, Japan. He is now with Mitsubishi Electric Company Ltd., Nagoya 461-8670, Japan (e-mail: inazuma_kazuya@hotmail.co.jp).

H. Utsugi was with the Department of Electrical Engineering, Nagaoka University of Technology, Nagaoka 940-2188, Japan. He is now with Sawafuji Electric Company Ltd., Oota 370-0344, Japan (e-mail: utg101-vault@ozzio.jp).

K. Ohishi and H. Haga are with the Department of Electrical Engineering, Nagaoka University of Technology, Nagaoka 940-2188, Japan (e-mail: ohishi@vos.nagaokaut.ac.jp; hagah@vos.nagaokaut.ac.jp).

Color versions of one or more of the figures in this paper are available online at http://ieeexplore.ieee.org.

Digital Object Identifier 10.1109/TIE.2012.2209610

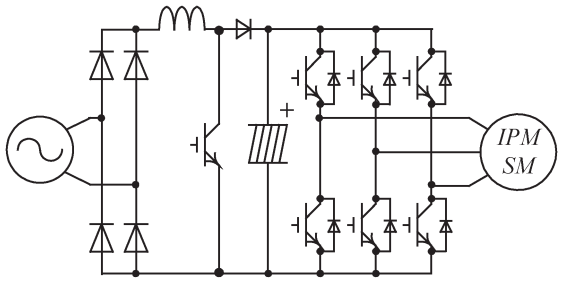

Fig. 1. Conventional single-phase-to-three-phase power converter.

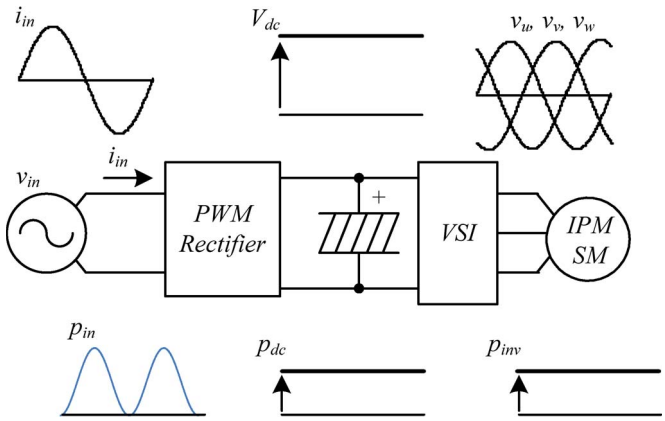

Fig. 2. Energy flow of the conventional converter.

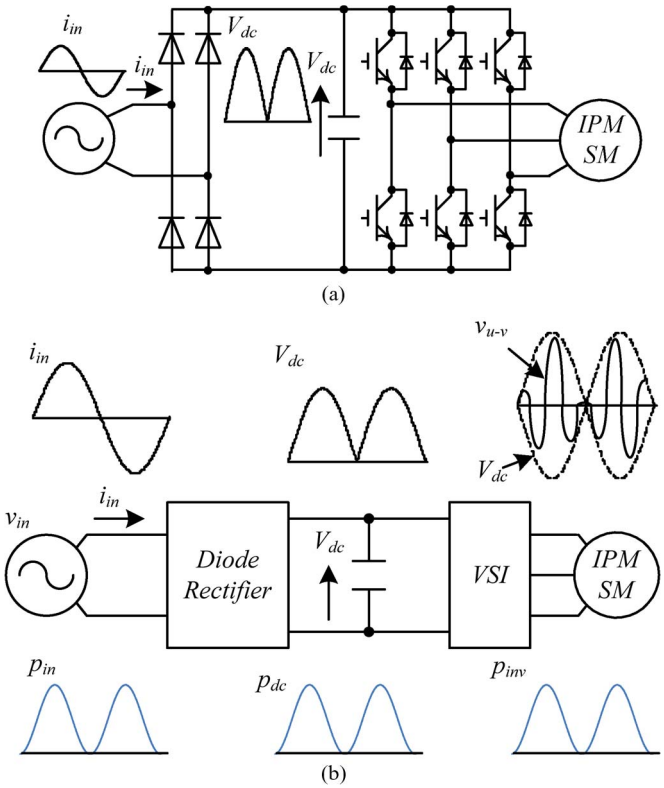

Fig. 3. Proposed power converter without electrolytic capacitor. (a) Power converter. (b) Energy flow.

the control method is significant because it has a lower part count than conventional motor drives. The proposed control method is that the inverter regulates $d-q$-axis current synchronous with the input voltage. The proposed control method is based on inverter output power for a q-axis current controller with a repetitive controller. Furthermore, in order to improve its power factor, the inverter also regulates the d-axis current synchronous with the input voltage. The validity of the proposed method is demonstrated experimentally, and its effectiveness is compared with that of the conventional method.

II. High-Power-Factor Power Converter Without Electrolytic Capacitor

A. Conventional Single-Phase-to-Three-Phase Power Converter

The most convenient scheme for ac-to-dc conversion, input power factor control, and output-voltage regulation is shown in Fig. 1. The source-side-current waveform is controlled by the boost chopper. The boost chopper obtains a sinusoidal current waveform using a reactor, an electrolytic capacitor, and a high-frequency switched power device. The reactor and capacitor are bulky and expensive. The power loss in the reactor is large. The capacitor determines the major lifetime-limiting factor of the power converter system. Moreover, in conventional systems, the loss in the power device is large, and it requires a noise filter. Fig. 2 shows the energy flow in the system. In the conventional system, the source-side ripple power is smoothed at the dc link by using a large-capacitance electrolytic capacitor. In this manner, the output power of the inverter is maintained constant.

A number of converter topologies have been reported in the literatures [18]–[24]. These circuits realize small size and high efficiency. However, these circuits also require reactors and switching devices.

In conventional approaches, high-power-factor operation is achieved by the rectifier along with the use of switching devices, a reactor, and an electrolytic capacitor. Inverter control and load-side motors have not been conventionally used for high-power-factor operation. The rectifier and inverter in a conventional system are separated by a dc link because of the bulky electrolytic capacitor. The single-phase ripple power is absorbed with the dc link to reduce torque ripple. A conventional inverter can control its output three-phase-voltage waveforms; however, it cannot control single-phase-source-current waveforms.

B. Proposed Single-Phase-to-Three-Phase Power Converter

Fig. 3 shows a schematic diagram of the proposed power converter, which consists of a single-phase diode rectifier, a small film capacitor, and a three-phase voltage-source inverter [25]–[27]. The film capacitor is used to absorb the dc-link current ripple due to the pulsewidth modulation (PWM) switching of the inverter. It consists of a few energy storage elements, and the single-phase power ripple is smoothed by the moment of inertia of the load motor.

In the proposed system, the inverter controller has the following two functions: It regulates the speed of the IPM motor, and it controls the source-side-current waveform to obtain high power factor of the single-phase diode rectifier. In Fig. 3(b), the

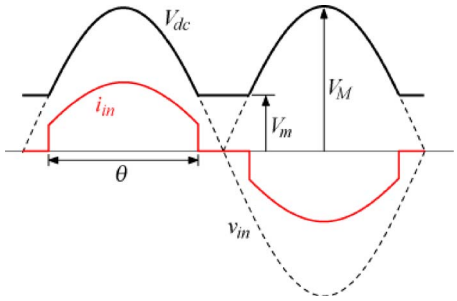

Fig. 4. Relationship between input current, input voltage, and dc-link voltage.

three-phase output power includes many ripple power synchronous with single-phase source voltage. The torque ripple appears at the IPM synchronous motor (IPMSM). Hence, the motor speed is regulated averagely.

Fig. 4 shows the principle of power factor improvement in the proposed system. A conventional capacitor-input-type diode rectifier with large electrolytic capacitors is used to maintain a constant dc-link voltage. Therefore, the diode conduction width is narrow, and the input power factor is low. The power factor of the proposed converter circuit (shown in Fig. 3) is improved by generating voltage ripples at the dc link. As shown in Fig. 4, the dc-link voltage $V_{\rm dc}$ generates ripples when a small film capacitor is used at the dc link, and the power factor is improved because of the broad diode conduction width. If the amplitude of $V_{\rm dc}$ is greater than the absolute value $|v_{\rm in}|$ of the input voltage, the input (grid) current $i_{\rm in}$ does not flow.

In Fig. 4, assuming that the input current is controlled in the manner of a sine wave section of the diode conduction width θ, the angles to become $i_{\rm in}=0$ are $(\pi-\theta)/2$ and $(\pi+\theta)/2$. Thus, the V_m is the voltage at these angles. When $v_{\rm in}$ is a sinusoidal waveform, θ can be obtained by the following equation:

$$\cos\left(\frac{\theta}{2}\right)=\frac{V_m}{V_M}. \tag{1}$$

In Fig. 4, effective power P is calculated by the following equation:

$$\begin{aligned}P&=\frac{1}{T}\int_0^T\{V_{\rm pk}\sin(\omega_{\rm in}t)\cdot I_{\rm pk}\sin(\omega_{\rm in}t)\}\,dt\\&=\frac{4}{T}\int_0^{T/4}\{V_{\rm pk}\sin(\omega_{\rm in}t)\cdot I_{\rm pk}\sin(\omega_{\rm in}t)\}\,dt\\&=\frac{4\cdot V_{\rm pk}\cdot I_{\rm pk}}{T}\int_{T(\pi-\theta)/4\pi}^{T/4}\{\sin^2(\omega_{\rm in}t)\}\,dt\\&=\frac{V_{\rm pk}\cdot I_{\rm pk}}{2\pi}(\theta+\sin\theta)\end{aligned} \tag{2}$$

where $V_{\rm pk}$ is the maximum voltage value and $I_{\rm pk}$ is the maximum current value. If $V_{\rm pk}=I_{\rm pk}=1$

$$P=\frac{1}{2\pi}(\theta+\sin\theta). \tag{3}$$

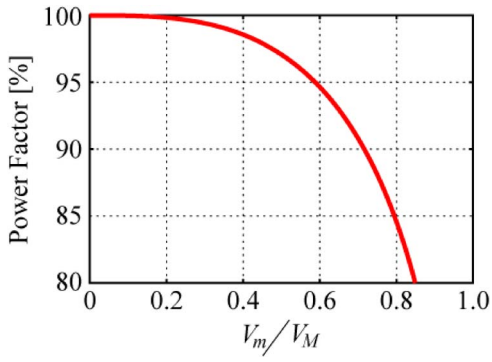

Fig. 5. Relationship between ripple ratio and power factor.

On the other hand, the rms value of current $I_{\rm rms}$ is calculated by the following equation:

$$\begin{aligned}\frac{I_{\rm rms}}{I_{\rm pk}}&=\sqrt{\frac{1}{T}\int_0^T\sin^2(\omega_{\rm in}t)dt}\\&=\sqrt{\frac{4}{T}\int_{(\pi-\theta)T/4\pi}^{\pi/4}\sin^2(\omega_{\rm in}t)dt}\\&=\sqrt{\frac{1}{2\pi}(\theta+\sin\theta)}.\end{aligned} \tag{4}$$

If $I_{\rm pk}=1$

$$I_{\rm rms}=\sqrt{\frac{1}{2\pi}(\theta+\sin\theta)}. \tag{5}$$

The input power factor $\cos\phi$ is calculated on the basis of the conduction width θ as follows:

$$\begin{aligned}\cos\phi&=\frac{P}{S}\\&=\frac{P}{V_{\rm rms}\cdot I_{\rm rms}}\\&=\frac{\frac{1}{2\pi}(\theta+\sin\theta)}{\frac{1}{\sqrt{2}}\cdot\sqrt{\frac{\theta+\sin\theta}{2\pi}}}\\&=\sqrt{\frac{\theta+\sin\theta}{\pi}}\end{aligned} \tag{6}$$

where S is the apparent power.

Fig. 5 shows the relationship between the input power factor and ratio V_m/V_M, whose definitions are given by (1) and (6). From Fig. 5, it is observed that a power factor of 95% or more can be obtained when $V_m/V_M<0.6$.

It is difficult to realize the proposed principle of power factor improvement. In the proposed system, the power factor improvement is realized by the switching devices at the inverter. Furthermore, the diode rectifier has nonlinear characteristic. Hence, it is difficult for the inverter to regulate the input current continually. It is also necessary for the inverter controller to regulate the motor current with twice the source frequency.

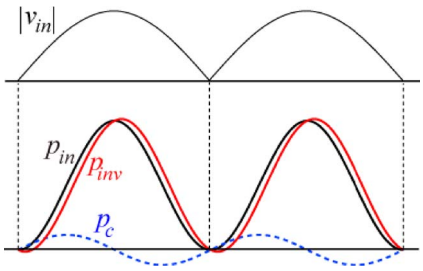

Fig. 6. Relationship between input power and output power of proposed system.

III. Inverter-Control Method for High Power Factor

A. Relationship of Input Current and Load Power

It is assumed that the instantaneous power in the load vibrates with a frequency twice that of the power supply frequency, which is given by (7) and (8) for synchronization with the input voltage

$$v_{\rm in} = V_{\rm pk} \sin \omega_{\rm in} t \tag{7}$$
$$p_{\rm load} = V_{\rm op} I_{\rm op} \sin^2 \omega_{\rm in} t \tag{8}$$

where $V_{\rm op}$ is the maximum output voltage and $I_{\rm op}$ is the maximum output current. The input current during this time becomes a sine wave with a unity power factor; the input current is as given by

$$i_{\rm in} = \frac{V_{\rm op} \cdot I_{\rm op}}{V_{\rm pk}} \sin \omega_{\rm in} t. \tag{9}$$

Therefore, to obtain a unity power factor, the instantaneous power of the load connected to the single-phase power supply must be controlled to ripple with twice the synchronized input-voltage frequency.

B. Feedback-Control Method for Inverter Output Power

In the circuit shown in Fig. 3, the relationship between the input power, dc-link capacitor power, and inverter output power is given by

$$p_{\rm in} = p_c + p_{\rm inv}. \tag{10}$$

Here, $p_{\rm in}$ denotes the input power, p_c denotes the dc-link capacitor power, and $p_{\rm inv}$ denotes the inverter output power. The relationship between each of these power components, for a unity input power factor, is shown in Fig. 6. In the proposed method, the inverter output power shows a high power factor; this is calculated using

$$p_{\rm inv} = v_d^* i_d + v_q^* i_q. \tag{11}$$

Here, v_d^* and v_q^* denote the d- and q-axis voltage references, and i_d and i_q denote the d- and q-axis currents, respectively. In the proposed method, the change in the inverter output power at the zero crossing of the input voltage is smooth and negligible, and the tracking performance of $p_{\rm inv}$ can be improved.

Fig. 7 shows the block diagram of the proposed system for controlling the inverter output power. The input power

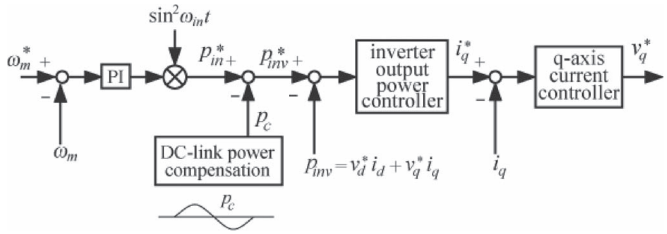

Fig. 7. Control block diagram of proposed system.

command $p_{\rm in}^*$ is determined by multiplying the output of the speed controller with the term $\sin^2 \omega_{\rm in} t$ generated from the input voltage $v_{\rm in} = V_{\rm in} \sin \omega_{\rm in} t$. The inverter-output-power command $p_{\rm inv}^*$ is calculated by subtracting the compensation power of the dc-link capacitor from the input power command $p_{\rm in}^*$, according to (10). The term p_c is calculated as follows.

If the $V_{\rm dc}$ is lower than zero

$$\begin{aligned} V_{\rm dc} &= V_{\rm pk} \left|\sin(\omega_{\rm in} t)\right| \\ &= V_{\rm pk} \sin(\omega_{\rm in} t) \cdot \operatorname{sgn}\left(\sin(\omega_{\rm in} t)\right) \end{aligned} \tag{12}$$

where $\operatorname{sgn}()$ is the sign function. The dc-link current i_c is calculated as follows:

$$\begin{aligned} i_c &= C_{\rm dc} \frac{dV_{\rm dc}}{dt} \\ &= C_{\rm dc} V_{\rm pk} \frac{d}{dt} \left\{\sin(\omega_{\rm in} t) \cdot \operatorname{sgn}(\sin(\omega_{\rm in} t))\right\} \\ &= \omega_{\rm in} C_{\rm dc} V_{\rm pk} \cos(\omega_{\rm in} t) \cdot \operatorname{sgn}\left(\sin(\omega_{\rm in} t)\right). \end{aligned} \tag{13}$$

Hence, p_c is calculated as follows:

$$\begin{aligned} p_c &= V_{\rm dc} \cdot i_c \\ &= \left\{V_{\rm pk} \sin(\omega_{\rm in} t) \cdot \operatorname{sgn}\left(\sin(\omega_{\rm in} t)\right)\right\} \\ &\quad \times \left\{\omega_{\rm in} C_{\rm dc} V_{\rm dc} \cos(\omega_{\rm in} t) \cdot \operatorname{sgn}\left(\sin(\omega_{\rm in} t)\right)\right\} \\ &= \omega_{\rm in} C_{\rm dc} V_{\rm pk}^2 \sin(\omega_{\rm in} t) \cos(\omega_{\rm in} t) \\ &= \frac{1}{2} \omega_{\rm in} C_{\rm dc} V_{\rm pk}^2 \sin(2\omega_{\rm in} t). \end{aligned} \tag{14}$$

The difference between $p_{\rm inv}^*$ and $p_{\rm inv}$ is the inverter-output-power error. This error is controlled by the inverter-output-power controller, and its output is the q-axis current command i_q^*. Thus, the input power factor is improved at light loads and low speeds on the basis of the inverter output power and the determination of i_q^*.

IV. d-Axis Current Control Synchronous With Source Voltage

A higher power factor is obtained when V_m is smaller and the ripple band of the dc-link voltage is larger, as shown in Fig. 4. The dc-link voltage increases because of the influence of the electromotive force when the motor speed increases. As a result, the input power factor decreases, and the current harmonic components increase. To solve this problem, the approximate value of the d-axis current is given by the flux-weakening-control method [28].

The well-known d-axis current control law for the flux weakening [28] can be applied to the proposed system. However, the power factor is low at any load condition. In this paper, the

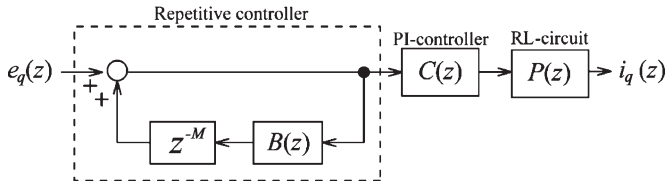

Fig. 8. q-axis current controller with repetitive controller.

TABLE I
MOTOR PARAMETER

Stator resistance R_a	0.866 [ohm]
d-axis inductance L_d	8 [mH]
q-axis inductance L_q	20 [mH]
Linkage flux ϕ_a	0.12 [wb]
Pole number	4 [pole]
Motor inertia	0.000576 [kgm^2]
Rated speed	4000 [rpm]
Rated torque	2.0 [Nm]

d-axis current command i_d^* is changed in synchronous with the source voltage to improve the input power factor as follows:

$$i_d^* = i_{\mathrm{dofs}} + A \cdot \sin(2\omega_{\mathrm{in}} \cdot t + \theta) \tag{15}$$

where the d-axis offset current i_{dofs} is the offset component of the i_d^*, A is the amplitude of the ripple component of i_d^*, and θ is the phase difference between the input voltage v_{in} and the ripple component of i_d^*. i_{dofs}, A, and θ are determined so that the proposed system obtains a high power factor in each operating condition. These values are adjusted by hand work for each operating condition. When motor speed is low, the flux-weakening-control method is also necessary because the dc-link voltage decrease is synchronous with the source voltage.

V. PROPOSED REPETITIVE CONTROLLER FOR INVERTER-OUTPUT-POWER CONTROL

Because the q-axis current command i_q^* serves as a frequency controller, it generally accompanies the response i_q in the proportional–integral (PI) controller used. Moreover, the proposed circuit does not contain energy storage elements; thus, the output-current control characteristics considerably influence the input characteristics. Therefore, controllers that can accurately control the output current to double the frequency band (100 Hz) at the power supply cycle (50 Hz) are required.

Fig. 8 shows the block diagram of a q-axis current controller with repetitive control with an error e_q between the q-axis current and the actual current i_q. The electrical model of the IPM motor is treated as an RL circuit $P(z)$ (where R is the stator resistance R_a and L is the q-axis inductance L_q in Table I) by using decoupling control, and the PI controller is denoted as $C(z)$. They are defined as follows:

$$P(z) = \frac{1}{R_a} \frac{1 - \exp\left(-\frac{1}{\tau_q} T_s\right)}{z - \exp\left(-\frac{1}{\tau_q} T_s\right)} \tag{16}$$

$$C(z) = K_q \left(1 + \frac{T_s}{T_i} \frac{1}{z-1}\right). \tag{17}$$

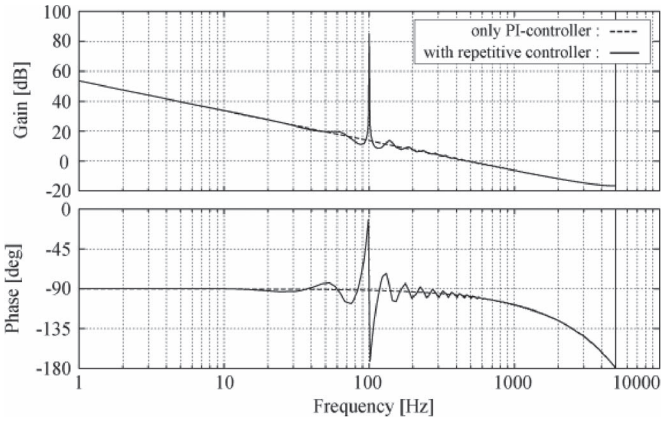

Fig. 9. Open-loop frequency of q-axis current controller.

Here, R_a denotes the stator resistance, τ_q denotes the q-axis circuit time constant, K_q denotes the proportional gain, T_i denotes the integral time, and T_s denotes the sampling period. The block $B(z)$ in Fig. 8 represents the bandpass filter, and this filter is defined as follows:

$$B(z) = \frac{b_0 z^2 + b_1 z + b_2}{a_0 z^2 + a_1 z + a_2}. \tag{18}$$

The filter is used to select the necessary frequency and secure the stability of the system. The central frequency of the bandpass filter is designed to be the input-power-ripple frequency. The number of delay steps M is calculated as $M = T_{\mathrm{in}}/T_s$, where T_{in} denotes the period of the input power.

Fig. 9 shows an example of the open-loop frequency response shown in Fig. 8. The input voltage frequency is 50 Hz, and the sampling frequency is 10 kHz. Therefore, the central frequency of the bandpass filter is selected as 100 Hz, which is equal to the input-power-ripple frequency; thus, M becomes 100. The short dashed line represents the conventional characteristics when only the PI control is used, and the solid line represents the characteristic of the PI control with the added repetitive control. The gain is understandably large, and thus, the control characteristics are fine for the input power ripple with a frequency of 100 Hz when the repetitive control is added.

VI. CONTROL BLOCK DIAGRAM

Fig. 10 shows the diagram of the entire circuit with the repetitive controller applied to the inverter-output-power controller. Control sensors are installed for the input power supplies v_{in}, the dc-link voltage V_{dc}, and the inverter output phase currents i_u and i_v. The proposed system has no additional current sensor to regulate the input-current waveform. The IPM motor is driven at the voltages v_u^*, v_v^*, and v_w^* based on vector control. For speed control, the error between the speed reference ω_m^* and the calculated speed ω_m is the input to the PI controller; ω_m is calculated by differentiating the rotor position obtained from the encoder. The output of the speed PI controller corresponds to the peak value of the input power required by the system.

The currents i_d and i_q obtained by coordinate conversion from the detected currents i_u and i_w, respectively, are

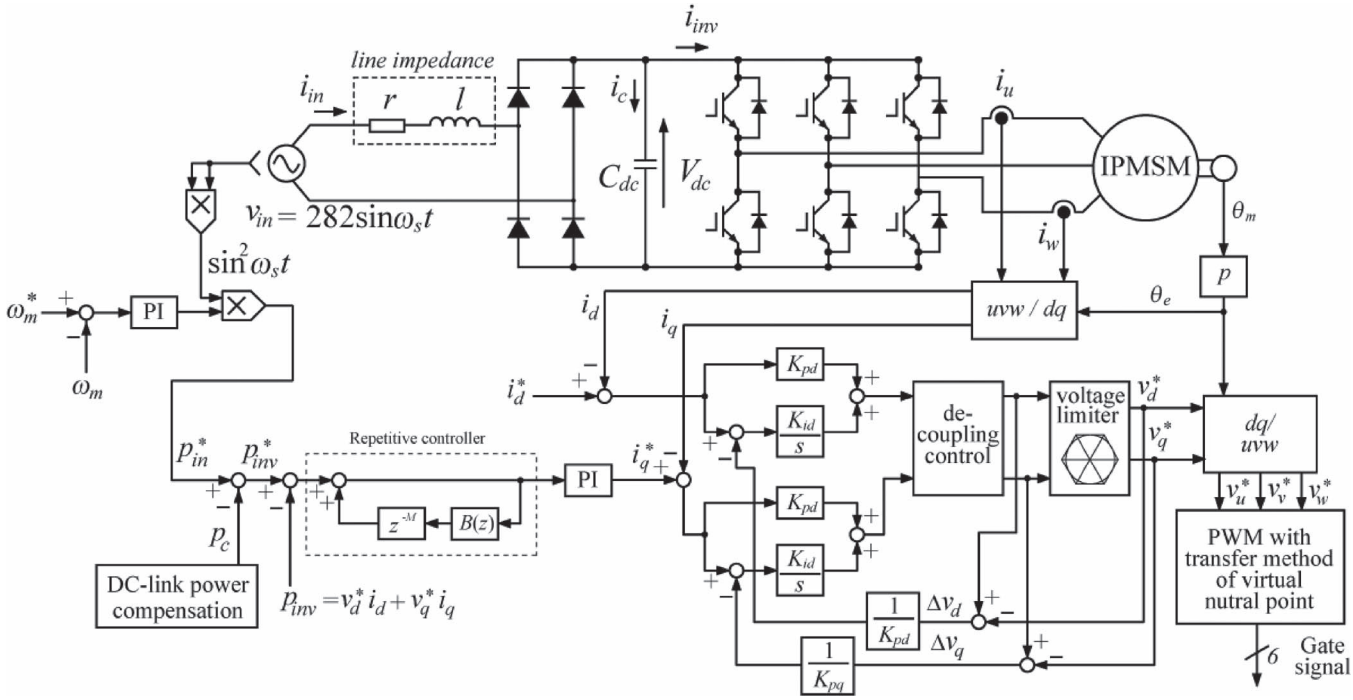

Fig. 10. Control block diagram of the proposed system.

subtracted from the reference currents i_d^* and i_q^*; each current is regulated by the PI controller. The voltage references are generated by the decoupled control outputs of the PI controllers.

In the proposed control system, the dc-link voltage varies synchronously with the input power supply. Because of the dc-link ripple voltage, the outputs of both d- and q-axis currents in the PI controllers are saturated. As a result, the source current $i_{\rm in}$ includes harmonic distortions. To improve the input-current waveform, this paper proposes a PI control method that accounts for the voltage limitations of the inverter [29]–[31] for the d- and q-axis currents.

Fig. 10 shows the block diagram of the proposed PI current controller with saturation feedback of d- and q-axis currents. When the output of the PI controller is saturated, it is calculated again using the values Δv_d and Δv_q obtained under saturated conditions. The voltage limitation value varies synchronously with the dc-link voltage $V_{\rm dc}$. Therefore, the proposed PI current controller operating with feedback using values obtained at saturation improves the input-current waveform because of the fine current regulation of the inverter. The inverter is operated by the modulation of these voltage references, and the IPM motor is driven.

VII. Experimental Results

The experimental results confirm our proposed control method. Table I lists the motor parameters for the tested IPMSM, and Table II lists the specifications for our proposed control system. The source voltage and frequency are set at 200 Vrms and 50 Hz, respectively. Line impedance is set at 0.2 mH and 0.5 Ω. These values are based on JISC61000-3-2 [32]. The tested IPMSM is connected to the generator. The

TABLE II
System Parameter

Input voltage	200 [Vrms]
Input frequency	50 [Hz]
Line impedance (l,r)	0.2 [mH], 0.5 [ohm]
DC-link capacitor C_d	14 [uF]
Carrier frequency	10 [kHz]
Control cycle	100 [usec]
Encoder pulse	2000 [pulse/rev]

experimental methods are introduced as follows. At first, the speed reference (constant value) is given to the controller. Next, the power supply increases the input voltage from zero to 200 Vrms.

Figs. 11–14 show the input voltages and the input currents of the experimental results of the conventional control method. The inverter-output-power controller of the conventional control method has only the PI controller, and the d-axis current reference is a constant value [33].

In the experiment, the rotor speeds were 2000 and 4000 r/min, and the load torques were 0.5 and 2.0 N · m.

Figs. 15–18 show the input voltages and input currents used for obtaining the experimental results of the proposed system. The inverter-output-power controller is the proposed repetitive control method; the d-axis current reference is synchronous with the source voltage. These figures also show the response of the inverter output power. In the control method with only the PI controller, the phase delay leads to a low power factor under light-load conditions, while in the proposed control method with the repetitive controller, the power factor is improved at any load conditions.

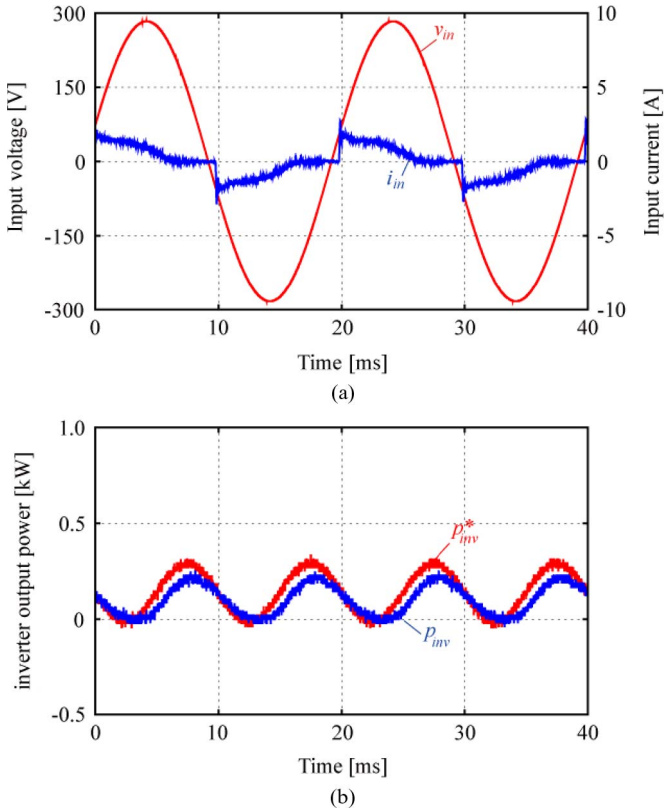

Fig. 11. Responses in the conventional control method (2000 r/min and 0.5 N · m).

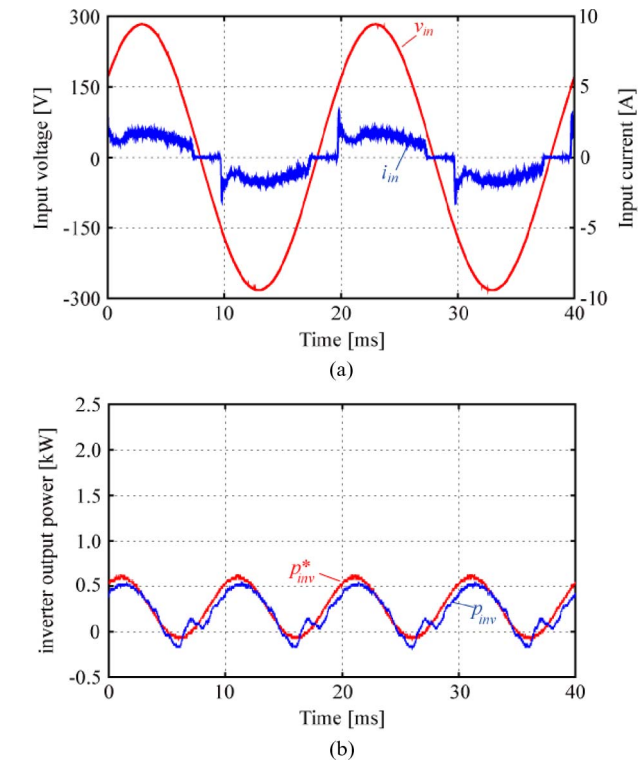

Fig. 12. Responses in the conventional control method (4000 r/min and 0.5 N · m).

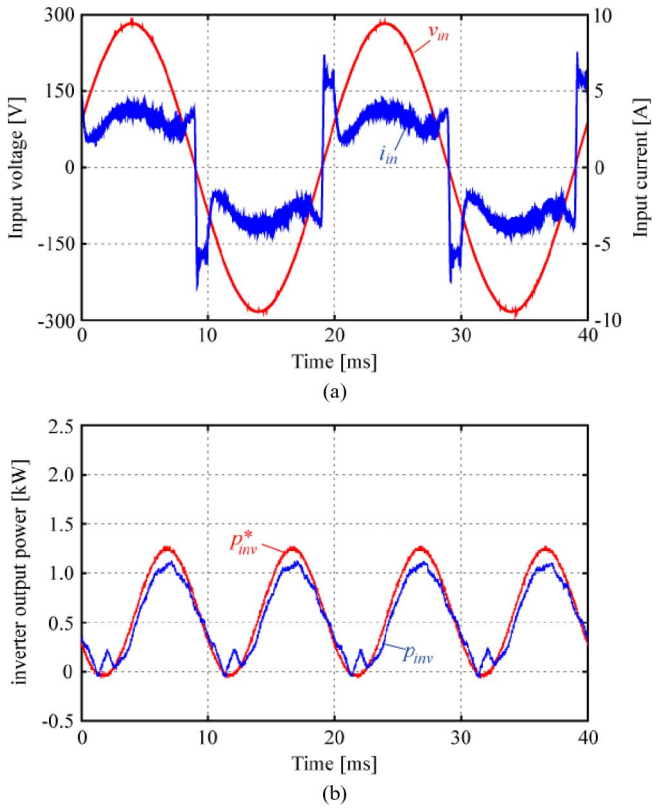

Fig. 13. Responses in the conventional control method (2000 r/min and 2.0 N · m).

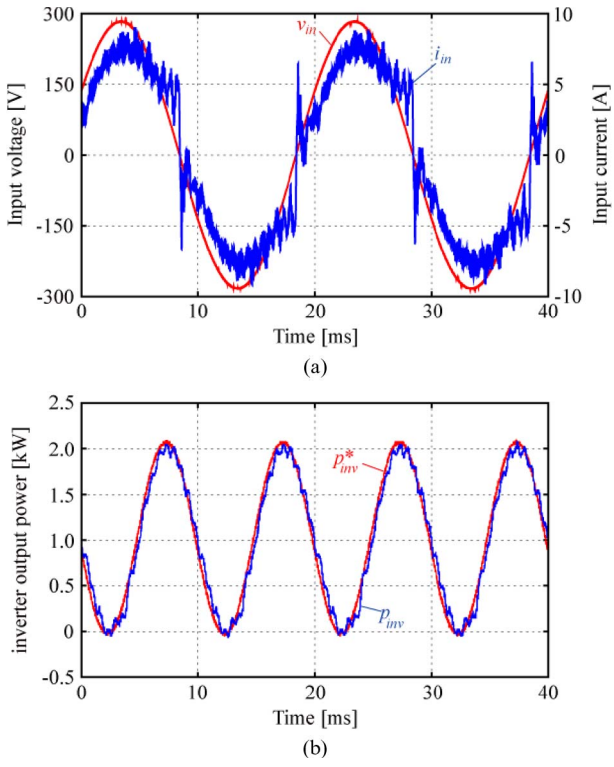

Fig. 14. Responses in the conventional control method (4000 r/min and 2.0 N · m).

Table III lists the input power factors of the experimental results. The conventional control method is the inverter-output-power control without the repetitive controller, and the d-axis current reference is a constant value [33]. Control method no. 1 is the inverter-output-power control without the repetitive controller, and the d-axis current reference has the sum of the

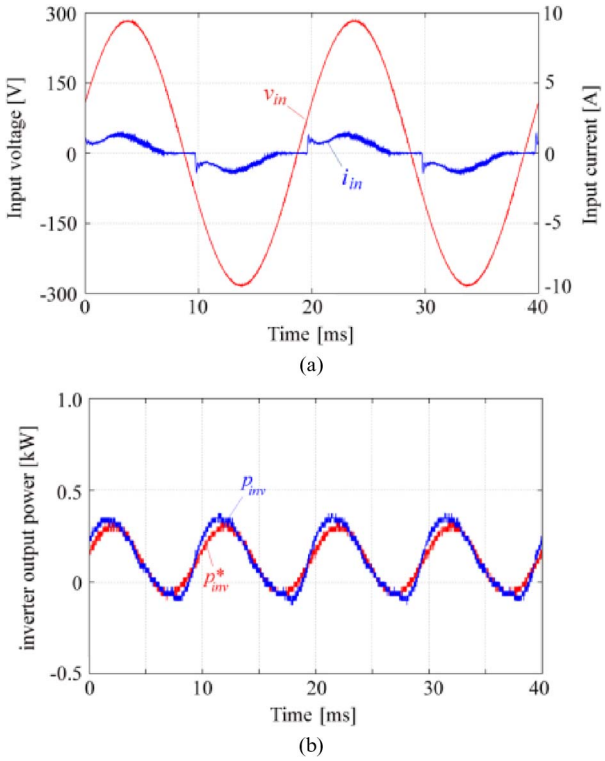

Fig. 15. Responses in the proposed control method (2000 r/min and 0.5 N·m).

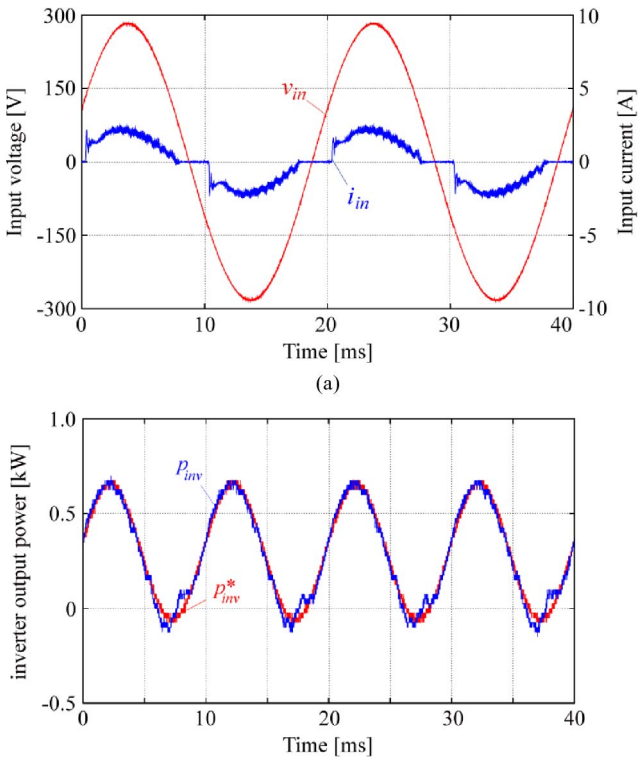

Fig. 16. Responses in the proposed control method (4000 r/min and 0.5 N·m).

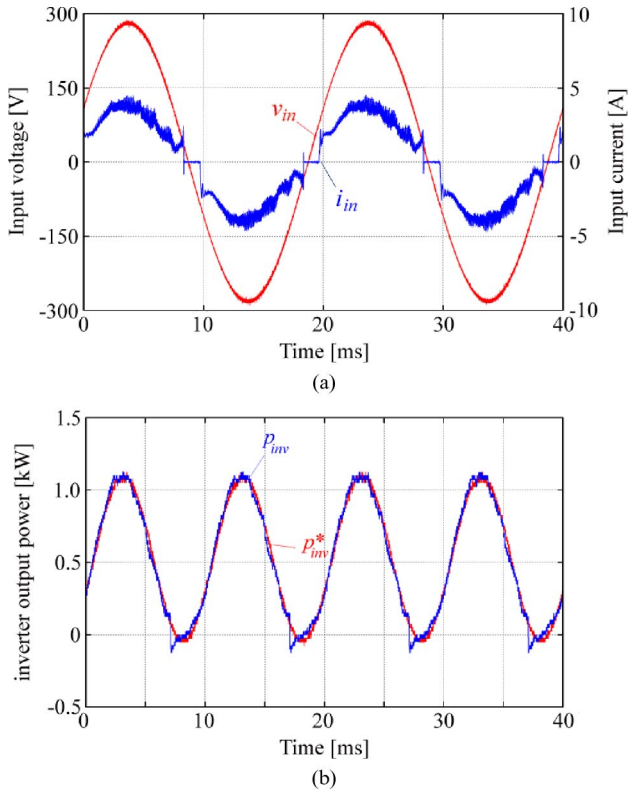

Fig. 17. Responses in the proposed control method (2000 r/min and 2.0 N·m).

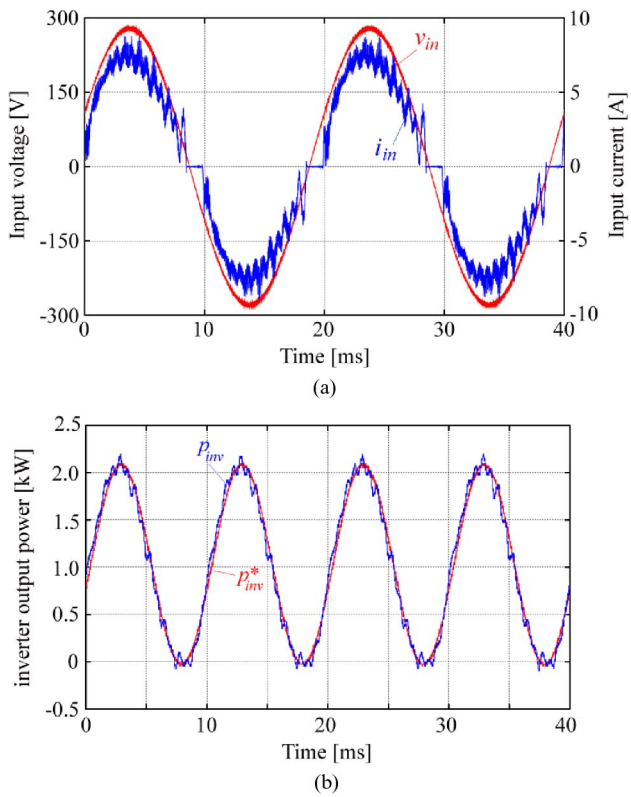

Fig. 18. Responses in the proposed control method (4000 r/min and 2.0 N·m).

constant value and fluctuation value. Control method no. 2 is the inverter-output-power control with the repetitive controller, and the d-axis current reference has only constant value. The proposed control method is the inverter-output-power control with the repetitive controller, and the d-axis current reference has the sum of the constant value and fluctuation value.

The power factor of control method no. 1 is higher than that of the conventional method on the condition of 2000 r/min and 2.0 N · m. The power factor of control method no. 2 is higher than that of the conventional method in any load condition.

TABLE III
COMPARISON OF INPUT POWER FACTOR

	Motor speed [rpm]	Load torque [Nm] 0.5	Load torque [Nm] 2
Conventional Control Method in [34] (q-axis: only PI, d-axis: only constant)	2000	85.4%	87.2%
	4000	96.7%	98.5%
Control Method no.1 (q-axis: only PI, d-axis: constant and fluctuation)	2000	80.1%	95.7%
	4000	96.5%	96.9%
Control Method no.2 (q-axis: with repetitive, d-axis: only constant)	2000	92.0%	98.5%
	4000	96.8%	98.5%
Proposed Control Method (q-axis: with repetitive, d-axis: constant and fluctuation)	2000	91.9%	98.7%
	4000	96.8%	98.7%

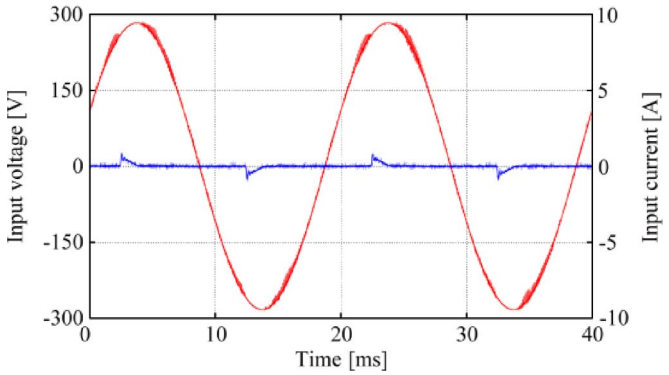

Fig. 19. Input-voltage and input-current waveforms (500 r/min and no-load condition).

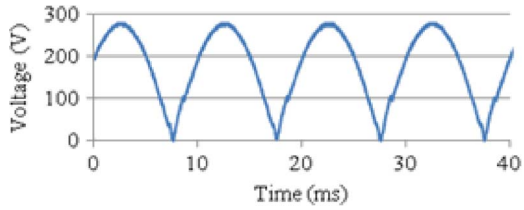

Fig. 20. DC-link voltage waveform (4000 r/min and 2 N · m).

Furthermore, the power factor of the proposed control method is higher than that of any control methods in any load condition.

The maximum power factor of the proposed method is 98.7% at the rated torque of 2.0 N · m. The proposed method with the inverter-output-power feedback achieves a high power factor under light-load conditions.

Fig. 19 shows the input voltage and input current used on the condition of 500 r/min and no load. In this case, the proposed controller also carries out the regulation of the motor speed.

Figs. 20 and 21 show the dc-link voltage waveforms for the proposed circuit. Fig. 20 shows the dc-link voltage at the rated-load conditions. The minimum dc-link voltage is reduced to approximately zero in spite of the motor's high-speed operation. Under the light-load condition shown in Fig. 21, the minimum dc-link voltage is also reduced by using the proposed control method.

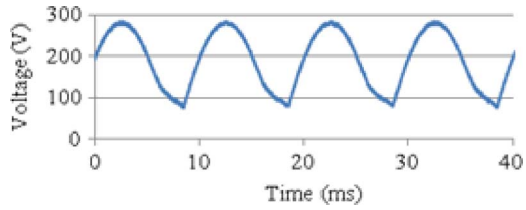

Fig. 21. DC-link voltage waveform (2000 r/min and 0.5 N · m).

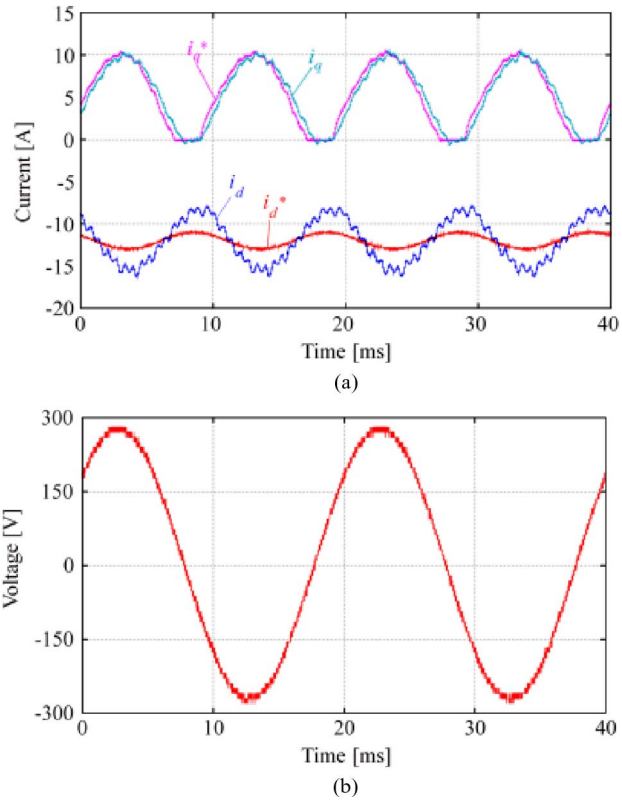

Fig. 22. d- and q-axis current waveforms.

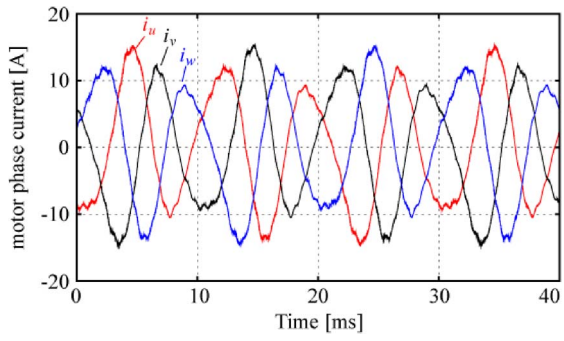

Fig. 23. Output-current waveforms.

Fig. 22 shows the d- and q-axis current waveforms for the proposed circuit. The bandwidth of the current regulator is set to 1500 rad/s. The d-axis current cannot follow the reference value because the d-axis current controller has no high gain controller such as the proposed repetitive controller.

Fig. 23 shows the output-current waveform for the proposed circuit. Fig. 24 shows the ripple component of the motor speed. Fig. 24(a) shows the ripple component by the proposed

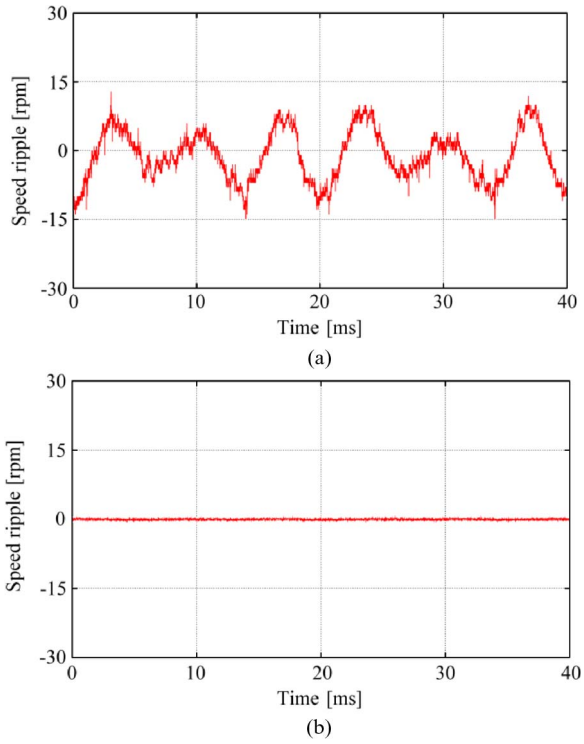

Fig. 24. Comparison of speed ripple component (4000 r/min and 2 N · m). (a) Proposed system. (b) Conventional system.

system without an electrolytic capacitor, and Fig. 24(b) shows the ripple component by the constant dc-link voltage with a huge electrolytic capacitor. The load motor is driven at the rated speed of 4000 r/min and the rated torque of 2.0 N · m. The output current has several ripples synchronized with the source voltage; the torque ripples are present in the IPM motor. Because of the moments of inertia of the motor and speed controller, the velocity of the IPM motor is smoothly regulated with some ripples. However, the proposed flux-weakening control is increasing in the inverter output current. Furthermore, the torque ripple is also increasing in the inverter output current. Hence, the motor efficiency of the proposed system is lower than that of the conventional constant dc-link voltage system. The motor efficiency of the proposed system is 86.2% at the rated speed of 4000 r/min and the rated torque of 2.0 N · m. The motor efficiency of the conventional system is 91.6% at the same condition.

VIII. Conclusion

This paper has proposed a new PFC method using an inverter-driven IPM motor. The proposed circuit realizes the high power factor of the single-phase diode rectifier by using three-phase inverter control and a load-side IPM motor. The proposed system consists of a diode rectifier, a three-phase inverter, and a small film capacitor at the dc link. The dc-link capacitance is 14 μF (0.33 J/kVA). It consists of a few energy storage elements, and the single-phase power ripple is smoothed by the moment of inertia of the load motor.

In addition, this paper has proposed a new inverter-control method in order to obtain a high power factor and achieve fine input-current waveform on the condition of both light load and rated load. The proposed control method is that the inverter regulates $d-q$ dual axis current synchronous with the input voltage. The proposed control method is based on the q-axis current controller for inverter output power with a repetitive controller. Furthermore, in order to improve its power factor, the inverter also regulates the d-axis current synchronous with the input voltage. A high power factor is obtained by regulating the inverter output power. The inverter-output-power controller is located between the speed controller and q-axis current controller.

The power factor of the proposed control method becomes higher than that of the conventional control methods. The maximum power factor obtained by the proposed method is 98.7% at the rated-load conditions. The effectiveness of the proposed method is proved experimentally by comparison with the conventional methods.

References

[1] J. Y. Chai, Y. H. Ho, Y. C. Chang, and C. M. Liaw, "On acoustic-noise-reduction control using random switching technique for switch-mode rectifiers in PMSM drive," *IEEE Trans. Ind. Electron.*, vol. 55, no. 3, pp. 1295–1309, Mar. 2008.

[2] F. J. T. E. Ferreira, J. A. C. Fong, and A. T. Almeida, "Ecoanalysis of variable-speed drives for flow regulation in pumping systems," *IEEE Trans. Ind. Electron.*, vol. 58, no. 6, pp. 2117–2125, Jun. 2011.

[3] E. C. Santos, C. B. Jacobina, G. A. A. Carlos, and I. S. Freitas, "Component minimized ac–dc–ac single-phase to three-phase four-wire converters," *IEEE Trans. Ind. Electron.*, vol. 58, no. 10, pp. 4624–4635, Oct. 2011.

[4] M. T. Madigan, R. W. Erickson, and E. H. Ismail, "Integrated high-quality rectifier-regulators," *IEEE Trans. Ind. Electron.*, vol. 46, no. 4, pp. 749–758, Aug. 1999.

[5] M. Daniele, P. K. Jain, and G. Joos, "A single-stage power-factor corrected ac/dc converter," *IEEE Trans. Power Electron.*, vol. 14, no. 6, pp. 1046–1055, Nov. 1999.

[6] Y.-C. Li and C.-L. Chen, "A novel single-stage high-power-factor ac-to-dc LED driving circuit with leakage inductance energy recycling," *IEEE Trans. Ind. Electron.*, vol. 59, no. 2, pp. 793–802, Feb. 2012.

[7] H. L. Cheng, Y. C. Hsieh, and C. S. Lin, "A novel single-stage high-power-factor ac/dc converter featuring high circuit efficiency," *IEEE Trans. Ind. Electron.*, vol. 58, no. 2, pp. 524–532, Feb. 2011.

[8] J. M. Alonso, J. Vina, D. G. Vaquero, G. Martinez, and R. Osorio, "Analysis and design of the integrated double buck–boost converter as a high-power-factor driver for power-LED lamps," *IEEE Trans. Ind. Electron.*, vol. 59, no. 4, pp. 1689–1697, Apr. 2012.

[9] Z. Li, C. Y. Park, J. M. Kwon, and B. H. Kwon, "High-power-factor single-stage LCC resonant inverter for liquid crystal display backlight," *IEEE Trans. Ind. Electron.*, vol. 58, no. 3, pp. 1008–1015, Mar. 2011.

[10] E. H. Ismail, A. J. Sabzali, and M. A. Al-Saffar, "A high-quality rectifier based on Sheppard–Taylor converter operation in discontinuous capacitor voltage mode," *IEEE Trans. Ind. Electron.*, vol. 55, no. 1, pp. 38–48, Jan. 2008.

[11] R.-L. Lin and C. Lo, "Design and implementation of novel single-stage charge-pump power-factor-correction electronic ballast for metal halide lamp," *IEEE Trans. Ind. Electron.*, vol. 59, no. 4, pp. 1789–1798, Apr. 2012.

[12] A. El Aroudi, M. Orabi, R. Haroun, and L. Martinez-Salamero, "Asymptotic slow-scale stability boundary of PFC ac–dc power converters: Theoretical prediction and experimental validation," *IEEE Trans. Ind. Electron.*, vol. 58, no. 8, pp. 3448–3460, Aug. 2011.

[13] R. Martinez and P. N. Enjeti, "A high-performance single-phase rectifier with input power factor correction," *IEEE Trans. Power Electron.*, vol. PE-11, no. 2, pp. 311–317, Mar. 1996.

[14] G. Moschopoulos and P. Jain, "A novel single-phase soft-switched rectifier with unity power factor and minimal component count," *IEEE Trans. Ind. Electron.*, vol. 51, no. 3, pp. 566–576, Jun. 2004.

[15] G. K. Andersen and F. Blaabjerg, "Current programmed control of a single-phase two-switch buck–boost power factor correction circuit," *IEEE Trans. Ind. Electron.*, vol. 53, no. 1, pp. 263–271, Feb. 2006.

[16] E. H. Ismail, A. J. Sabzali, and M. A. Al-Saffar, "Buck–boost-type unity power factor rectifier with extended voltage conversion ratio," *IEEE Trans. Ind. Electron.*, vol. 55, no. 3, pp. 1123–1132, Mar. 2008.
[17] E. H. Ismail, "Bridgeless SEPIC rectifier with unity power factor and reduced conduction losses," *IEEE Trans. Ind. Electron.*, vol. 56, no. 4, pp. 1147–1157, Apr. 2009.
[18] X. Liu, P. Wang, P. C. Loh, and F. Blaabjerg, "A compact three-phase single-input/dual-output matrix converter," *IEEE Trans. Ind. Electron.*, vol. 59, no. 1, pp. 6–16, Jan. 2012.
[19] J. Ebrahimi, E. Babaei, and G. B. Gharehpetian, "A new multilevel converter topology with reduced number of power electronic components," *IEEE Trans. Ind. Electron.*, vol. 59, no. 2, pp. 655–667, Feb. 2012.
[20] L. Li and Q. Zhong, "Novel zeta-mode three-level AC direct converter," *IEEE Trans. Ind. Electron.*, vol. 59, no. 2, pp. 897–903, Feb. 2012.
[21] J. Jung, S. Lim, and K. Nam, "A feedback linearizing control scheme for a PWM converter-inverter having a very small dc-link capacitor," *IEEE Trans. Ind. Appl.*, vol. 35, no. 5, pp. 1124–1131, Sep./Oct. 1999.
[22] C. B. Jacobina, T. M. Oliveira, and E. R. C. da Silva, "Control of the single-phase three-leg ac/ac converter," *IEEE Trans. Ind. Electron.*, vol. 53, no. 2, pp. 467–476, Apr. 2006.
[23] M. E. Ortuzar, R. E. Carmi, J. W. Dixon, and L. Moran, "Voltage-source active power filter based on multilevel converter and ultracapacitor dc link," *IEEE Trans. Ind. Electron.*, vol. 53, no. 2, pp. 477–485, Apr. 2006.
[24] D.-C. Lee and Y.-S. Kim, "Control of single-phase-to-three-phase ac/dc/ac PWM converters for induction motor drives," *IEEE Trans. Ind. Electron.*, vol. 54, no. 2, pp. 797–804, Apr. 2007.
[25] I. Takahashi and H. Haga, "Direct torque IPM motor control method to obtain unity power factor using a single-phase diode rectifier," in *Proc. IEEE. IEMDC*, 2003, vol. 2, pp. 1078–1083.
[26] H. Lamsahel and P. Mutschler, "Permanent magnet drives with reduced DC-link capacitor for home appliances," in *Proc. 35rd Annu. Conf. IEEE IECON*, 2009, pp. 725–730.
[27] T. Yokoyama, K. Ohishi, H. Haga, and J. Shibata, "Control method for achieving high power factor in single-phase to three-phase converters without electrolytic capacitors," (in Japanese), *Trans. IEEJ*, vol. 129-D, no. 5, pp. 490–497, 2009.
[28] S. Morimoto, Y. Takeda, T. Hirasa, and K. Taniguchi, "Expansion of operating limits for permanent magnet motor by current vector control considering inverter capacity," *IEEE Trans. Power Electron.*, vol. 26, no. 5, pp. 866–871, Sep./Oct. 1990.
[29] M. Sazawa, K. Ohishi, and S. Katsura, "Robust high speed position servo system considering current & voltage limitation and load inertia variation," in *Proc. 33rd Annu. Conf. IEEE IECON*, 2007, pp. 322–327.
[30] J. S. Hu, K. Y. Chen, T. Y. Shen, and C. H. Tang, "Control of voltage source inverter using multidimensional feedback quantization modulator," *IEEE Trans. Ind. Electron.*, vol. 58, no. 7, pp. 3027–3036, Jul. 2011.
[31] H. B. Shin and J. G. Park, "Anti-windup PID controller with integral state predictor for variable-speed motor drives," *IEEE Trans. Ind. Electron.*, vol. 59, no. 3, pp. 1509–1516, Mar. 2012.
[32] "Electromagnetic compatibility (EMC)-Part 3-2: Limits-limits for harmonic current emissions (equipment input current $<$ 20 A per phase)," (in Japanese) JISC61000-3-2, 2003. [Online]. Available: http://www.jisc.go.jp/
[33] K. Inazuma, K. Ohishi, and H. Haga, "High-power-factor control for inverter output power of IPM motor driven by inverter system without electrolytic capacitor," in *Proc. IEEE ISIE*, 2011, pp. 619–624.

Kazuya Inazuma received the B.E. degree in electrical, electronics, and information engineering from the Sendai National College of Technology, Sendai, Japan, in 2009 and the M.E. degree in electrical, electronics, and information engineering from the Department of Electrical Engineering, Nagaoka University of Technology, Nagaoka, Japan, in 2011.

He is currently with Mitsubishi Electric Company Ltd., Nagoya, Japan. His research interests include power electronics.

Hiroaki Utsugi received the B.E. degree in electrical engineering from Gunma National College of Technology, Maebashi, Japan, in 2010 and the M.E. degree in electrical, electronics, and information engineering from the Department of Electrical Engineering, Nagaoka University of Technology, Nagaoka, Japan, in 2012.

He is currently with Sawafuji Electric Company Ltd., Oota, Japan. His research interests include power electronics.

Kiyoshi Ohishi (M'86–SM'08) received the B.E., M.E., and Ph.D. degrees in electrical engineering from Keio University, Yokohama, Japan, in 1981, 1983, and 1986, respectively.

From 1986 to 1993, he was an Associate Professor with the Osaka Institute of Technology, Osaka, Japan. Since 1993, he has been with the Department of Electrical Engineering, Nagaoka University of Technology, Nagaoka, Japan, where he has been a Professor since 2003. His research interests include power electronics, mechatronics, and motion control.

Dr. Ohishi was the recipient of the Outstanding Paper Awards at the 1985 IEEE International Conference on Industrial Electronics, Control, and Instrumentation (IECON) and the Best Paper Awards at IECON 2002 and IECON 2004 from the IEEE Industrial Electronics Society. He was also the recipient of the Best Paper Award from the Institute of Electrical Engineers of Japan in 2002.

Hitoshi Haga (M'08) received the B.E., M.E., and D.Eng. degrees in energy and environmental science from the Nagaoka University of Technology, Nagaoka, Japan, in 1999, 2001, and 2004, respectively.

From 2004 to 2007, he was a Researcher with Daikin Industries, Ltd., Osaka, Japan. From 2007 to 2010, he was an Assistant Professor with the Sendai National College of Technology, Sendai, Japan. Since 2010, he has been with the Department of Electrical Engineering, Nagaoka University of Technology. His research interests include power electronics.